RSC Advances

ROYAL SOCIETY OF CHEMISTRY

www.rsc.org/advances

Journal Name

ARTICLE

Enhancement of performance and sulfur resistance of ceria-doped V/Sb/Ti with sulfation for selective catalytic reduction of NOx with ammonia

Received 00th January 20xx,
Accepted 00th January 20xx

DOI: 10.1039/x0xx00000x

www.rsc.org/

Dong Wook Kwon and Sung Chang Hong*

Ceria-doped V/Sb/Ti catalyst prepared with sulfation was investigated for the selective catalytic reduction of NOx by NH_3. Sulfation treatment was carried out at 250, 300, 400, and 500 °C. The properties of the catalysts were studied using physico-chemical analyses, including Brunauer-Emmett-Teller (BET) surface area analysis, X-ray photoelectron spectroscopy (XPS), H_2 temperature-programmed reduction (H_2-TPR), temperature programmed oxidation (TPO), NH_3 and NO temperature programmed desorption (TPD), transmission infrared spectra (IR), and thermal gravimetric analysis (TGA). Sulfated catalyst demonstrated increased activity due to the following causes: i) total acidity was increased by the formation of SO_4^{2-}–NH_4^+ on the surface of the catalyst; ii) fast SCR reaction was induced by the production of NO_2 through reaction of NO and O_2; iii) the excellent SCR activity can be attributed to an enhancement in active oxygen species and chemisorption of NH_3. SCR reaction over sulfated CeO_2 mainly enhanced the Eley-Rideal mechanism as compared to the V/Sb/Ce/Ti (Fresh). Sulfated catalyst demonstrated the best catalytic activity when sulfation was carried out at 500 °C for 1 h. At the same time, SO_2 resistant was also observed to be increased. For increasing sulfation time, further increase in catalytic activity was not observed. In contrast, SO_2 resistance was decreased with prolonged sulfation. Sulfated ceria had positive effects on the catalytic activity; however, if formed at higher than appropriate levels, negative effects were observed on SO_2 deactivation. When considering the activity and SO_2 deactivation for ceria-doped V/Sb/Ti catalyst, the optimal conditions for sulfation were 500 °C for 1 h.

Introduction

The selective catalytic reduction (SCR) of NOx with NH_3 is well known to be the best available control technology for cleaning flue gases in terms of removal efficiency, stability, and economics[1]. In this process, the NOx contained in flue gases is reduced to N_2 and H_2O by NH_3.

Many metal oxide based catalysts, such as V_2O_5-WO_3/TiO_2 [2], Cu/TiO_2 [3], Fe/TiO_2 [4], and Mn/TiO_2 [5] have also been widely studied. Among these catalysts, the vanadium-titania based catalyst has been a widely accepted commercial catalyst. However, this type of catalyst is efficient only within the narrow temperature window of 300–400 °C. Considering these disadvantages, many researchers have continued to modify the current catalysts and develop novel vanadium catalysts which contain other metal elements. Huang et al.[6] reported high sulfur resistance with increased activity when Cr was added into the V_2O_5/TiO_2 catalyst. Zhang et al.[7] increased the activity at low temperatures by using an F-doped V_2O_5-WO_3/TiO_2 catalyst. According to Ha et al.[8], Sb at 2 wt.% showed stronger SO_2 resistant than 10 wt.% tungsten due to high electrical conductivity.

The ceria (CeO_2) has received considerable attention for NH_3-SCR to promote NOx conversion at low temperatures. Ceria has been extensively studied due to its oxygen storage and redox properties[9]. This compound can store and release oxygen via the redox shift between Ce^{4+} and Ce^{3+} under oxidizing and reducing conditions, respectively[10]. Ceria mixed oxide catalysts, such as CeO_2/TiO_2 [11], CeO_2-WO_3 [12], CeO_2-WO_3/TiO_2 [13], Ce-Cu-Ti oxides[14], and Mn-Ce/TiO_2 [15], have shown excellent catalytic activity and N_2 selectivity at 300–400 °C. In addition, the sulfation treatment for enhancement of the SCR activity has been used. According to Baraket et al.[16], the sulfation generates Lewis and Brönsted acidity at the surface and improves the redox properties due to the existence of strong electronic interaction between vanadia and sulfates in the V_2O_5/TiO_2 catalysts. Guo et al.[17] reported that sulfated V_2O_5/TiO_2 indicate excellent catalytic activity because it increases the Brönsted acid sites. Amiridis et al.[18] also reported that the gaseous SO_2 can mainly participate to the formation of surface sulfate species on V_2O_5/TiO_2 catalyst which strongly interact with vanadia and improve the catalytic surface reactivity. Furthermore, sulfated ceria catalysts were demonstrated to have clearly increased activity in the SCR reaction[19]. Sulfated ceria was present in two types: cerium (III) sulfates and cerium (IV) sulfates[20]. However, the cause of the

Department of Environmental Energy Engineering, Graduate School of Kyonggi University, 94-6 San, Iui-dong, Youngtong-ku, Suwon-si, Gyeonggi-do 443-760, Republic of Korea. E-mail: schong@kgu.ac.kr; Fax: (+82)31-2544941
† Electronic Supplementary Information (ESI) available. See
DOI: 10.1039/x0xx00000x

increase in activity of sulfated ceria has not been clearly identified. Several claims have been made regarding the increase in activity of sulfated ceria. First, it was stated that the positive effect of sulfated ceria is most probably due to the formation of more cerium (III) sulfates[21]. On the other hand, Chang et al. reported that the sulfate species were located on the cerium (IV) sulfates of the CeO_2 catalyst[22]. As such, the state of the sulfated ceria in ceria mixed oxide catalysts has yet to be resolved. In particular, the investigation on the optimal sulfation conditions and SO_2 resistance properties of sulfated catalysts for SCR activity enhancement is needed.

Recently, catalyst composed by a V/Sb/Ce/Ti mixed oxide had shown excellent activity and SO_2 resistance at low temperature[23]. The influence of SO_2 on the V/Sb/Ce/Ti oxide catalyst was found to be very interesting. The SO_2 resistance increased due to the addition of ceria, and the $Ce_2(SO_4)_3$ from SO_2 was formed. Due to the fact that the presence of SO_2 is unavoidable in the SCR reaction atmosphere, the influence of sulfate on the V/Sb/Ce/Ti oxide catalyst is worthy of studying. Hence, it is important to understand the effects of sulfation on the catalytic activity, the reaction pathway and the characteristics of SO_2 resistance induced by the sulfated ceria. The aim of the present was to identify the changes in Ce valence state caused by sulfate of V/Sb/Ti catalyst with addition of Ce, and the causes for the increase in activity. In addition, we aimed to derive the optimal sulfation conditions for conferring high SO_2 resistance. This study was focused particularly on the mechanisms of sulfation for increased catalytic activity and SO_2 resistance. In the present study, Brunauer-Emmett-Teller (BET) surface area analysis, X-ray photoelectron spectroscopy (XPS), H_2 temperature-programmed reduction (H_2-TPR), temperature programmed oxdiation (TPO), NH_3 and NO temperature programmed desorption (TPD), transmission infrared spectra (IR), and thermal gravimetric analysis (TGA) methods were used to characterize the catalysts and confirm the surface/bulk sulfate species.

Results and discussion

NH_3-SCR activity of catalysts.

The catalytic activity of the V/W/Ti, V/Sb/Ti, and V/Sb/Ce/Ti catalysts in the presence and absence of SO_2 is shown in Fig. 1(a). The reaction conditions were as follows: 750 ppm NO, 48 ppm NO_2, NH_3/NOx=1.0, 3 vol.% O_2, 6 vol.% H_2O, 800 ppm SO_2 (when used),

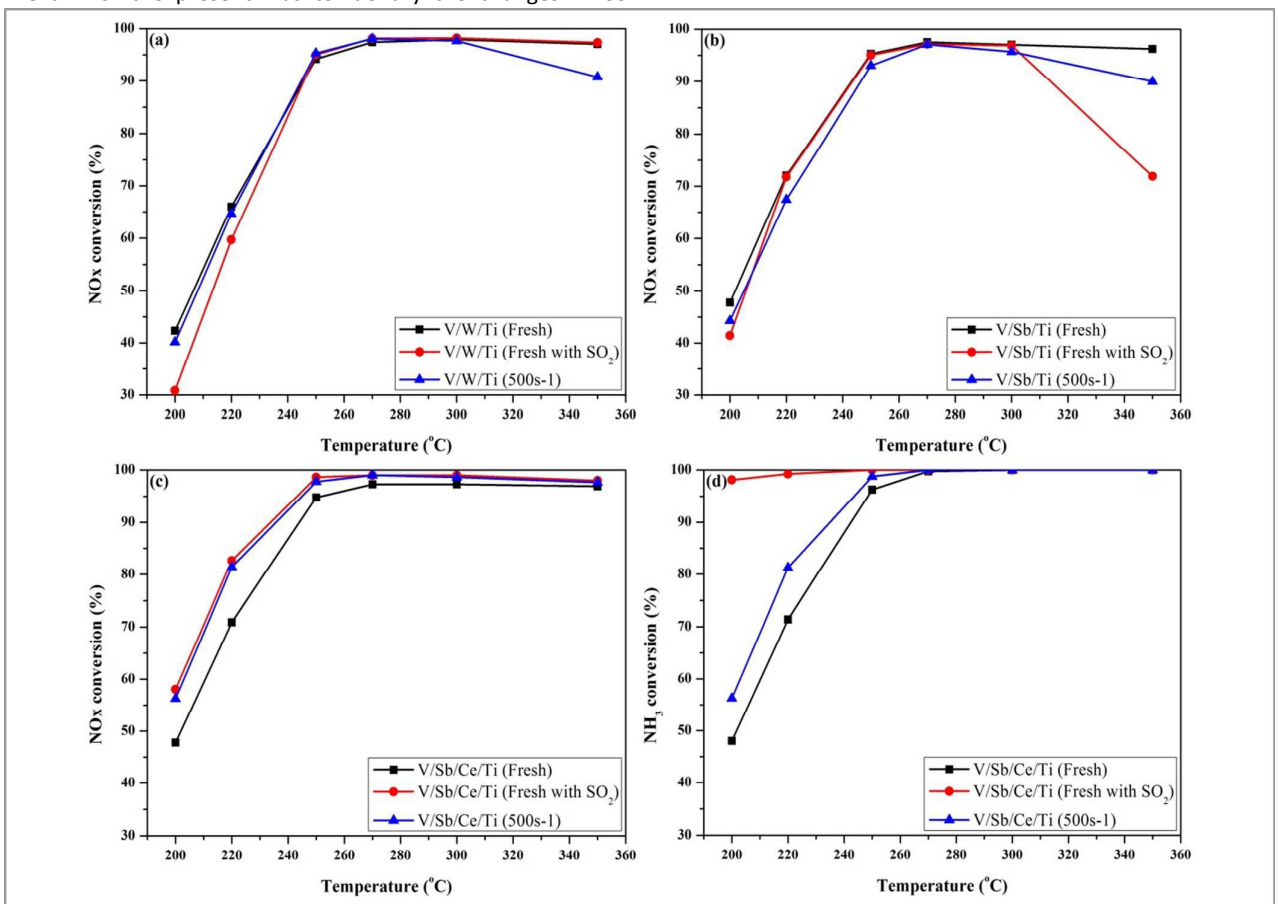

Fig. 1 The effect of reaction temperature on (a) NOx conversion of V/W/Ti, (b) NOx conversion of V/Sb/Ti, (c) NOx conversion of V/Sb/Ce/Ti, and (d) NH_3 conversion of V/Sb/Ce/Ti (NO: 750 ppm, NO_2: 48 ppm, NH_3/NOx: 1.0, SO_2 : 800 ppm (with SO_2), O_2: 3 vol.%, H_2O: 6 vol.%, GHSV: 60,000 h^{-1}).

total flow rate 600 cc/min at 200–350 °C, and the gas hourly space velocity (GHSV) was 60,000 h^{-1}. The effect of sulfur in the V/W/Ti

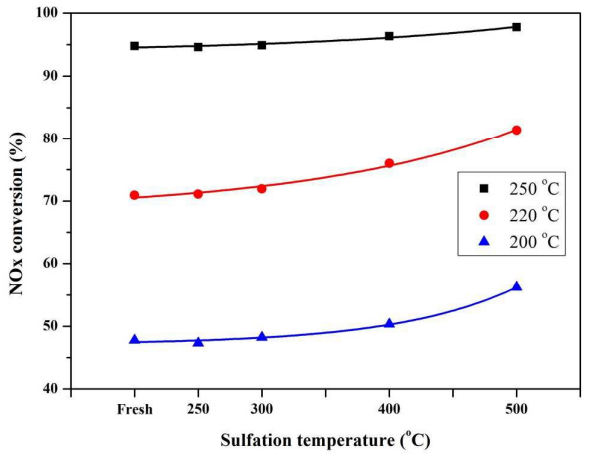

Fig. 2 The effect of sulfation temperature on NOx conversion of V/Sb/Ce/Ti catalysts (NO: 750 ppm, NO_2: 48 ppm, NH_3/NOx: 1.0, O_2: 3 vol.%, H_2O: 6 vol.%, GHSV: 60,000 h^{-1}).

catalyst known as a representative commercial catalyst was examined. NOx conversion over the V/W/Ti (Fresh with SO_2) decreased 11.5% at 200 °C as compared to the V/W/Ti (Fresh). In the case of V/W/Ti (500s-1), the catalytic activity has been lowered at 300 °C or higher. In the SCR reaction of V/Sb/Ti (Fresh with SO_2), the catalytic activity was severely decreased at 300 °C or higher. The activity of V/Sb/Ti (500s-1) was decreased similar to the V/W/Ti (500s-1). V/W/Ti and V/Sb/Ti catalysts are considered that there is no enhancement of the SCR activity by the sulfation. It shows a negative effect when the sulfur was present in the V/W/Ti and V/Sb/Ti catalysts that does not contain ceria. On the other hand, NOx conversion over the V/Sb/Ce/Ti (Fresh with SO_2) increased 10.3% at 200 °C as compared to the V/Sb/Ce/Ti (Fresh) (Fig. 1(c)). The NOx conversion over the V/Sb/Ce/Ti catalyst was confirmed to have an obvious increase as 500 ppm of SO_2 was introduced. This indicated obvious promotion of the catalytic activity of the added ceria catalyst due to the presence of SO_2. As is well known, SO_2 can react with metal oxides resulting in sulfation[24]. The SCR reaction of V/Sb/Ce/Ti (500s-1) was studied to examine the increase in efficiency caused by SO_2 in the SCR reaction through the addition of ceria. It can be seen in Fig. 1(c) that the catalytic activity of V/Sb/Ce/Ti (500s-1) was obviously promoted over sulfated ceria. During the SCR reaction over all catalysts, only a small amount of N_2O was formed (N_2 selectivity was higher than 99%). Fig. 1(d) shows the NH_3 conversion during the SCR reaction. NH_3 conversion

Table 1 The surface area, S/Ti ratio, Ce^{3+} ratio, and O_α ratio by XPS of various catalysts.

Catalyst	S_{BET} (m^2/g)	S/Ti ratio by XPS[a]	Ce^{3+} ratio (%)[a]	O_α ratio (%)[a]
V/Sb/Ce/Ti (Fresh)	67.2	-	23.42	38.25
V/Sb/Ce/Ti (250s-1)	65.6	0.075	29.12	38.55
V/Sb/Ce/Ti (300s-1)	62.6	0.085	34.34	44.11
V/Sb/Ce/Ti (400s-1)	63.0	0.130	41.47	44.48
V/Sb/Ce/Ti (500s-1)	58.0	0.164	47.16	55.37

[a] Surface atomic ratio calculated from XPS data.

increased in the following order: V/Sb/Ce/Ti (Fresh) < V/Sb/Ce/Ti (500s-1) < V/Sb/Ce/Ti (Fresh) with SO_2, which was consistent with the sequence of NOx conversion. V/Sb/Ce/Ti (Fresh) with SO_2 showed a very high NH_3 conversion of more than 98% at 200 °C. The reason was that unreacted ammonia formed $(NH_4)_2SO_4$ by reacting with SO_2 and H_2O after SCR reactions performed at temperatures lower than 220 °C[25].

The experiments were performed using sulfated catalysts prepared at various sulfation temperatures to examine the influence of sulfation temperature on the selective catalytic reduction activity. As shown in Fig. 2, the catalytic activity was measured for the V/Sb/Ce/Ti (Fresh), V/Sb/Ce/Ti (250s-1), V/Sb/Ce/Ti (300s-1), V/Sb/Ce/Ti (400s-1), and V/Sb/Ce/Ti (500s-1). In the case of the V/Sb/Ce/Ti (250s-1), increase in activity was not observed, while the activity of the V/Sb/Ce/Ti (300s-1) increased very little. In contrast, the V/Sb/Ce/Ti (400s-1) and V/Sb/Ce/Ti (500s-1) showed increase in activity at temperatures less than 250 °C. When V/Sb/Ce/Ti (Fresh) was treated with sulfation at 500 °C for 1 h, it showed higher activity than that of sulfation at less than 500 °C. The surface areas of the V/Sb/Ce/Ti (Fresh), V/Sb/Ce/Ti (250s-1), V/Sb/Ce/Ti (300s-1), V/Sb/Ce/Ti (400s-1), and V/Sb/Ce/Ti (500s-1) are collated in Table 1, where the values were 67.2, 65.6, 62.6, 63.0, and 58.0 m^2/g, respectively. The surface area was highest for V/Sb/Ce/Ti (Fresh). With sulfation of V/Sb/Ce/Ti catalysts at 500 °C, the surface area slightly decreased due to the sulfation at relatively high temperature.

Characterization of catalysts with sulfate.

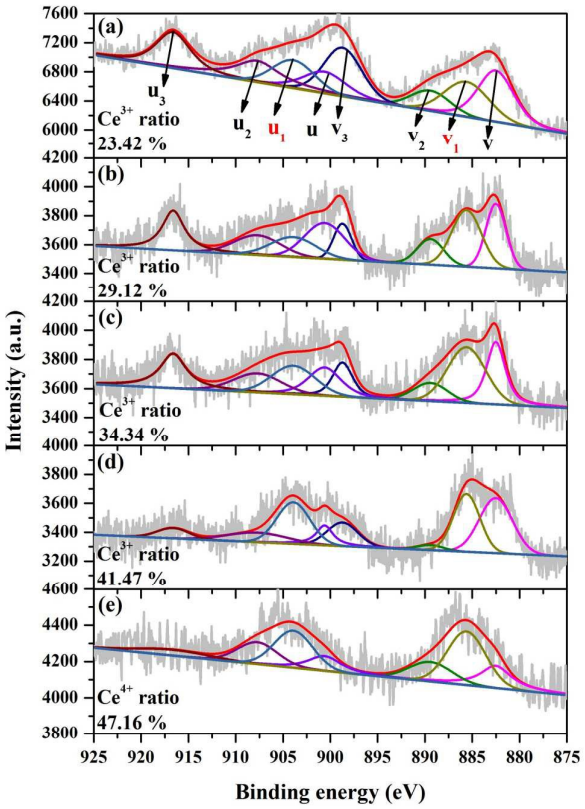

Fig. 3 The Ce 3d peaks of the V/Sb/Ce/Ti (Fresh) and sulfated V/Sb/Ce/Ti catalysts by XPS.

Sulfated catalyst showed various activities based on the sulfation temperature. We predicted that the catalysts would show various characteristics depending on the sulfation temperature. XPS analysis of the V/Sb/Ce/Ti (Fresh) and sulfated V/Sb/Ce/Ti were performed. The Ce 3d peak was also fitted into sub-bands by searching for the optimum combination of Gaussian bands. The sub-bands labeled u_1 and v_1 represented the $3d^{10}4f^1$ initial electronic state corresponding to Ce^{3+}, while the sub-bands labeled u, u_2, u_3, v, v_2, and v_3 represented the $3d^{10}4f^0$ state of Ce^{4+} [13]. The Ce^{3+} ratio (%) was calculated by $Ce^{3+}/(Ce^{3+} + Ce^{4+})$ of the V/Sb/Ce/Ti (Fresh). The Ce 3d peaks of the V/Sb/Ce/Ti catalysts by XPS are shown in Fig. 3. The Ce^{3+} ratio (%) was also shown to increase with sulfation temperature, in the following order: V/Sb/Ce/Ti (500s-1) (47.16%) > V/Sb/Ce/Ti (400s-1) (41.47%) > V/Sb/Ce/Ti (300s-1) (34.34%) > V/Sb/Ce/Ti (250s-1) (29.12%) > V/Sb/Ce/Ti (Fresh) (23.42%). The Ce^{3+} ratio was increased with the increase in sulfation temperature, which was caused by the increase of $Ce_2(SO_4)_3$. The increase of $Ce_2(SO_4)_3$ can be explained by the increase of the S/Ti ratio on the surface of the catalyst (Table 1). TPO analysis was performed on the sulfated catalyst to examine the amount of sulfur formed on the surface of the catalyst in more detail. SO_2 (m/z=64) signals were confirmed. Fig. 4 shows the peak observed around 600 and 850 °C for sulfated catalysts. Xu et al.[20] claimed that the peak occurring at 700–875 °C corresponded to sulfated ceria species as the result of SO_2-TPD of Ce/Ti. In the present study, it was thought that CeO_2 formed $Ce_2(SO_4)_3$ by reaction with SO_2 in the V/Sb/Ce/Ti (Fresh).

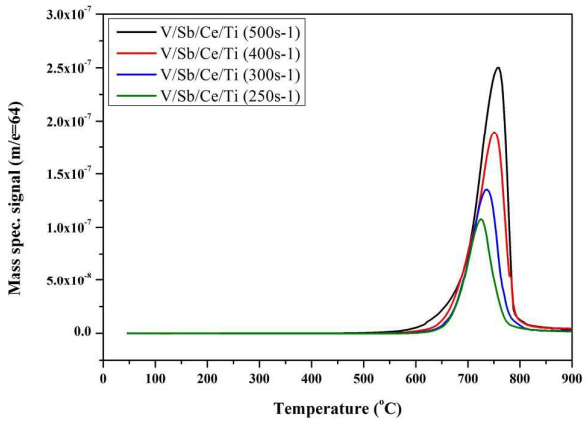

Fig. 4 TPO profiles of sulfated V/Sb/Ce/Ti catalysts (Experimental conditions: 30 mg cat, 21% O_2/Ar oxidation with heating rate 10 °C /min, total flow rate 50 cm^3/min).

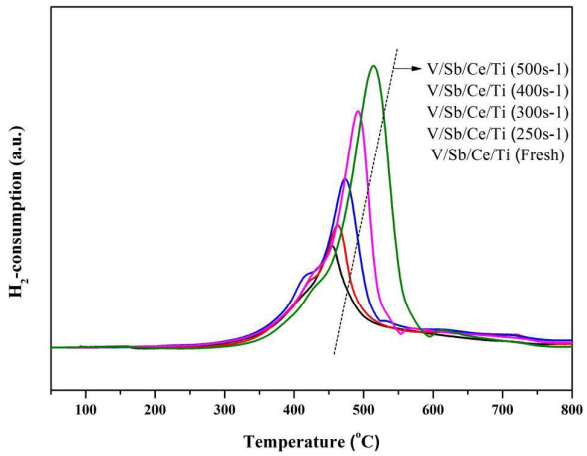

Fig. 5 H_2-TPR profiles of V/Sb/Ce/Ti (Fresh) and sulfated V/Sb/Ce/Ti catalysts (Experimental conditions: 30 mg cat, pretreatment at 400 °C for 30 min with 5% O_2/Ar 50 cm^3/min, 10% H_2/Ar reduction with heating rate 10 °C /min, total flow rate 50 cm^3/min).

H_2-TPR analysis was carried out to investigate the presence of reducible species in V/Sb/Ce/Ti catalysts as a function of sulfation temperature. Fig. 5 shows the results of the H_2-TPR analysis for V/Sb/Ce/Ti (Fresh), V/Sb/Ce/Ti (250s-1), V/Sb/Ce/Ti (300s-1), V/Sb/Ce/Ti (400s-1), and V/Sb/Ce/Ti (500s-1). All catalysts exhibited major reduction peaks at temperatures in the range of 300–600 °C. The V/Sb/Ce/Ti (Fresh) showed the peak of maximum reducing temperature (T_{max}) at 453 °C, which could be assigned to the reduction of surface vanadia, antimony, and ceria species[26]. The reduction peaks of 380–403 °C are attributed to vanadium species, and the reduction peak of 426 °C correspond to SbOx species. The TPR peak at approximately 450 °C could be ascribed to the surface reduction of CeOx species. These reduction peaks were attributed to the reductions from V^{5+} to V^{3+}, Sb^{5+} to Sb^{3+}, and Ce^{4+} to Ce^{3+} in the catalytic surface. A new peak at a temperature of 461 °C was observed for the V/Sb/Ce/Ti (250s-1). Upon the increase of sulfation temperature, V/Sb/Ce/Ti (500s-1) exhibited peak of T_{max} other than V/Sb/Ce/Ti (Fresh) (453 °C), (V/Sb/Ce/Ti (250s-1)

(461 °C), V/Sb/Ce/Ti (300s-1) (472 °C), and V/Sb/Ce/Ti (400s-1) (492 °C) at higher temperature. Since SO_4^{2-} species were reduced at a higher temperature than the surface reduction of Ce^{4+} to Ce^{3+} [19], the peak at 461 °C could possibly be caused by SO_4^{2-}. In addition, the peaks of each catalysts were different. The H_2-consumption (μmol/g) of V/Sb/Ce/Ti catalysts were also shown to increase with sulfation temperature, in the following order: V/Sb/Ce/Ti (500s-1) (1,881) > V/Sb/Ce/Ti (400s-1) (1,569) > V/Sb/Ce/T (300s-1) (1,388) > V/Sb/Ce/Ti (250s-1) (977) > V/Sb/Ce/Ti (Fresh) (861). The S/Ti ratio by XPS (Table 1) and TPO result (Fig. 4) reveal that the peak of T_{max} at 514 °C increased in V/Sb/Ce/Ti (500s-1) with the highest amount of SO_4^{2-}. Thus, a higher SO_4^{2-} was beneficial for the catalytic efficiency of V/Sb/Ce/Ti and occurred when the sulfation temperature of catalysts was 500 °C.

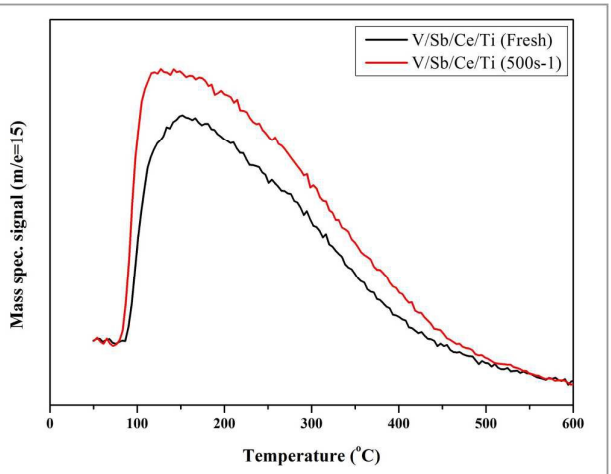

Fig. 6 NH_3-TPD patterns of V/Sb/Ce/Ti (Fresh) and V/Sb/Ce/Ti (500s-1).

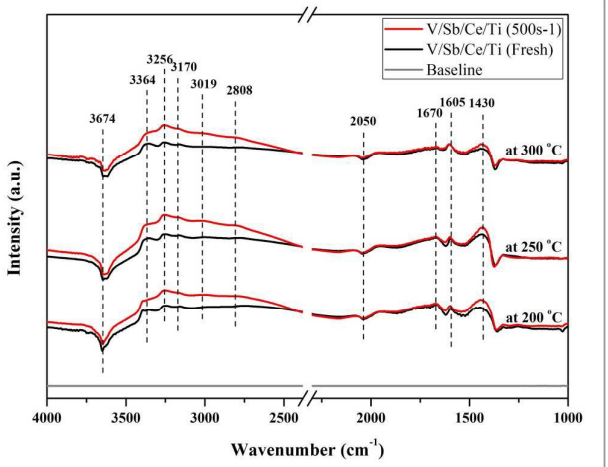

Fig. 7 DRIFTs spectra of V/Sb/Ce/Ti (Fresh) and V/Sb/Ce/Ti (500s-1) exposed to 1,000 ppm NH_3 for 0.5 h at 200, 250, and 300 °C.

The effects of the $Ce_2(SO_4)_3$ species formed by sulfation on NH_3 adsorption capacity were also examined. The adsorption abilities of the catalysts were measured with NH_3-TPD and NH_3-DRIFTs analysis. NH_3-TPD was measured to examine the acid site of the catalysts in the SCR reaction. The NH_3-TPD curves of V/Sb/Ce/Ti (Fresh) and V/Sb/Ce/Ti (500s-1) are shown in Fig. 6. All catalysts contained two broad NH_3 desorption peaks at 80–200 and 230–500 °C, which were attributed to the Brönsted and Lewis acid sites, respectively. Ammonia adsorbed on Brönsted acid sites is well known to desorb at lower temperatures than on Lewis acid sites[27]. The results of NH_3-TPD analysis revealed that the desorption peak was the largest in the temperature range of 80–500 °C for the V/Sb/Ce/Ti (500s-1). The area of the peaks at NH_3-TPD were as follows (ratio of the area was indicated): V/Sb/Ce/Ti (500s-1) (1.00) > V/Sb/Ce/Ti (Fresh) (0.75) catalyst.

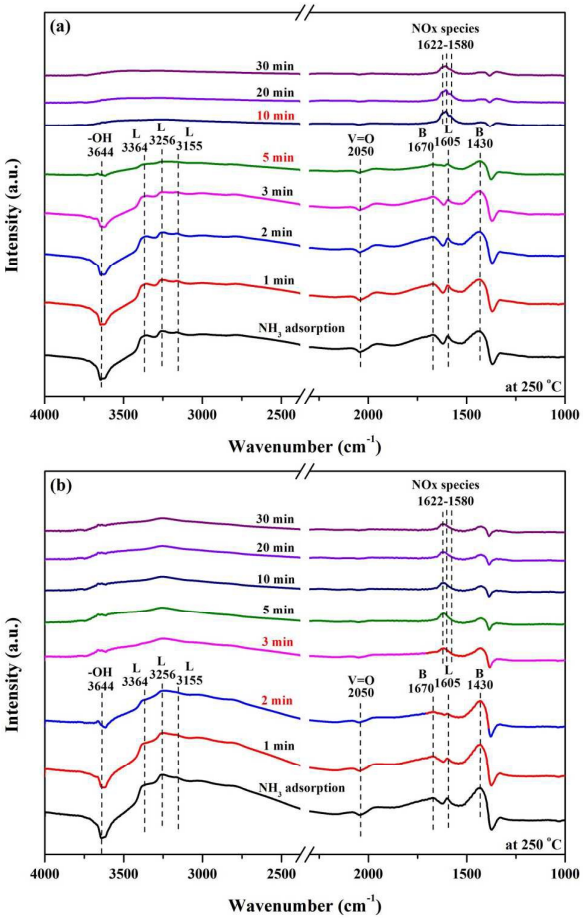

Fig. 8 DRIFT spectra of (a) taken at 250 °C upon passing 1,000 ppm NO + 3% O_2 over the NH_3 pre-adsorbed on V/Sb/Ce/Ti (Fresh) for 0, 1, 2, 3, 5, 10, 20, and 30 min, (b) taken at 250 °C upon passing 1,000 ppm NO + 3% O_2 over the NH_3 pre-adsorbed on V/Sb/Ce/Ti (500s-1) for 0, 1, 2, 3, 5, 10, 20, and 30 min.

To further determine the effects of NH_3 adsorption on the SCR reaction, NH_3 adsorption analysis was performed using a DRIFT spectrometer at 200, 250, and 300 °C to show the differences of catalytic activity. The results are shown in Fig. 7. NH_3 at 1,000 ppm was injected for 0.5 h, and the adsorbed species were measured. In these experiments, the peak corresponding to –OH, caused by the adsorption of NH^{4+} onto –OH, was observed at 3674 cm^{-1}, while the adsorption of NH_3 on the Lewis acid sites was observed at 1605, 3170, 3256, and 3364 cm^{-1} [28]. For all catalysts, peaks corresponding to the –OH and Lewis acid sites were observed. In all cases, a negative peak was also observed at 2050 cm^{-1}, corresponding to V=O[29]. In addition, the adsorption of the NH^{4+} ion on the Brönsted acid sites was simultaneously observed at 1430 and 1670 cm^{-1} [28]. The Lewis acid and Brönsted acid sites were found to be increased in the V/Sb/Ce/Ti (500s-1) in comparison with the V/Sb/Ce/Ti (Fresh). After sulfation, the increase in acid sites (Lewis acid and Brönsted acid sites) improved the NH_3 adsorption ability[16]. In this study, the total acidity was increased as SO_4^{2-}–NH^{4+} was formed by the adsorption of $NH_{3(g)}$ in SO_4^{2-} formed by sulfation. The SO_4^{2-}–NH^{4+} was activated into SO_4^{2-}–NH_2. Consequently, as it reacted with $NO_{(g)}$, it was converted into N_2 and H_2O[19].

The V/Sb/Ce/Ti (Fresh) was purged with NH_3 for 0.5 h, and NO + O_2/Ar was then introduced into the IR at 250 °C, and the spectra were recorded as a function of time (Fig. 8(a)). After NO + O_2/Ar had been injected, the peaks of the ammonia species decreased. In the case of V/Sb/Ce/Ti (Fresh), the peaks of the ammonia species decreased after 10 min. At the same time, new bands were detected at 1622 to 1580 cm^{-1} that could be attributed to the NOx species[30]. When compared to V/Sb/Ce/Ti (Fresh), the peaks assigned to the adsorbed ammonia species decreased more quickly on for the V/Sb/Ce/Ti (500s-1) (Fig. 8(b)). When the catalyst was purged with NO + O_2/Ar for only 3 min, all of the peaks resulting from ammonia species decreased. At the same time, new bands were detected at 1622 to 1580 cm^{-1} that could be attributed to NOx species[31]. On the basis of Fig. 8(a,b), it could be concluded that NOx readily reacted with the adsorbed ammonia species, especially for the V/Sb/Ce/Ti (500s-1).

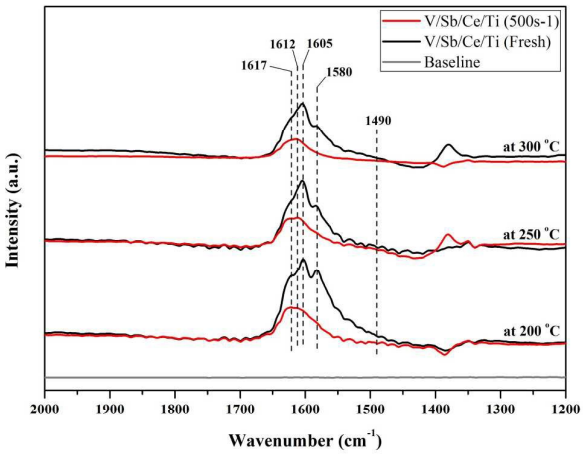

Fig. 9 DRIFT spectra of the adsorption of NO + O_2/Ar over V/Sb/Ce/Ti (Fresh) and V/Sb/Ce/Ti (500s-1) at 200, 250, and 300 °C.

Fig. 9 shows the DRIFT spectra of the adsorption of NO + O_2/Ar on V/Sb/Ce/Ti (Fresh) and V/Sb/Ce/Ti (500s-1) at 200, 250, and 300 °C. The characteristic vibration of NO + O_2/Ar adsorption on V/Sb/Ce/Ti catalysts mainly appeared at about 1617, 1612, 1605, 1580, and 1490 cm^{-1}. The band at 1617 cm^{-1} could be assigned to NO_2 [31], and the bands at 1612, 1605 (1580), and 1490 cm^{-1} could be assigned to bridged nitrate, bidentate nitrate, and monodentate nitrate, respectively[32]. In the case of catalyst V/Sb/Ce/Ti (500s-1), the intensity of the adsorption of NO + O_2/Ar was much less than that on V/Sb/Ce/Ti (Fresh). In addition, at 200 °C, the V/Sb/Ce/Ti (500s-1) shows a main peak of adsorption at 1617 cm^{-1} which corresponding to NO_2. Whereas, the V/Sb/Ce/Ti (Fresh) exhibits a main peak of absorption at 1605, 1612, and 1579 cm^{-1} corresponding to the bridged nitrate and bidentate nitrate. Liu et at.[33] reported that the monodentate nitrate, the bridge nitrate, and the bidentate nitrate are NO adsorbed species, which are inert in SCR reaction. Furthermore, according to Chen et al.[32], at low temperatures, the adsorbed NO_2 is the SCR reaction proceeds by reaction with NH_3. Thus, V/Sb/Ce/Ti (500s-1) showing a main peak of adsorption in the NO_2 exhibits a better activity than V/Sb/Ce/Ti (Fresh) at a low temperature.

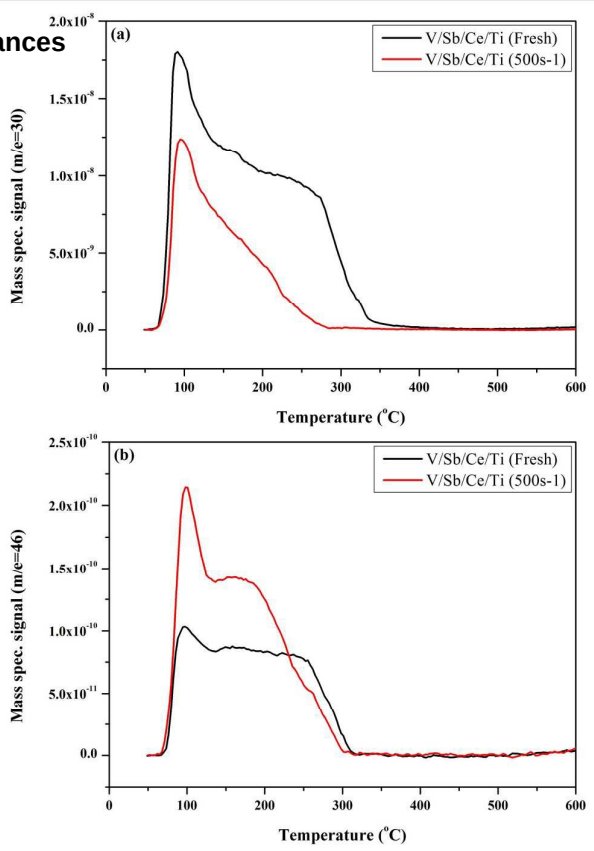

Fig. 10 NO-TPD patterns of V/Sb/Ce/Ti (Fresh) and V/Sb/Ce/Ti (500s-1): (a) peaks of NO, (b) peaks of NO_2.

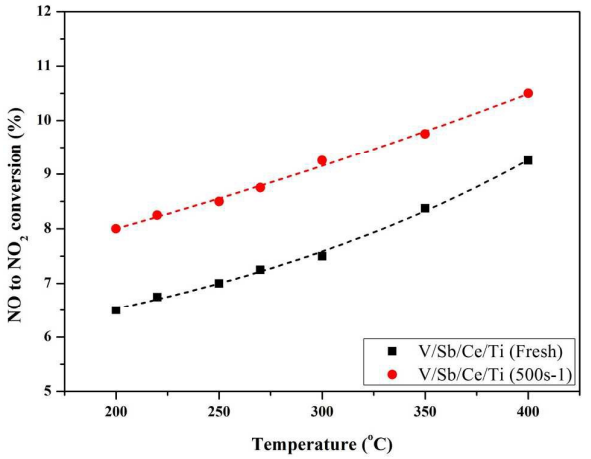

Fig. 11 Effect of reaction temperature on NO to NO_2 conversion of V/Sb/Ce/Ti (Fresh) and V/Sb/Ce/Ti (500s-1) (NO: 750 ppm, NO_2: 48 ppm, O_2: 3 vol.%, H_2O: 6 vol.%, GHSV: 60,000 h^{-1}).

The results of NO-TPD analysis of the V/Sb/Ce/Ti (Fresh) and V/Sb/Ce/Ti (500s-1) are reported in Fig. 10. The NO desorption spectrum of V/Sb/Ce/Ti (Fresh) and V/Sb/Ce/Ti (500s-1) are shown in Fig. 10(a). The NO desorption spectrum of the V/Sb/Ce/Ti (Fresh) showed three peaks at 95, 170, and 270 °C. Only two peak at 95 and 170 °C were found in the NO desorption spectrum of V/Sb/Ce/Ti (500s-1). The ratio of the peak area of NO of was 2.32 : 1.00 (Fresh : 500s-1), indicating that the NO desorption peak of V/Sb/Ce/Ti (Fresh) was larger than the NO desorption peak of V/Sb/Ce/Ti (500s-1). In Fig. 10(b), the NO_2 desorption spectrum of V/Sb/Ce/Ti (Fresh) and V/Sb/Ce/Ti (500s-1). The ratio of the area of NO_2 peaks was 1.00 : 1.40 (Fresh : 500s-1). Unlike the NO desorption spectrum,

the NO_2 desorption peak of the V/Sb/Ce/Ti (500s-1) was larger than the NO desorption peak of the V/Sb/Ce/Ti (Fresh). The desorbed NO_2 on the catalysts was from the decomposition of the intermediates formed after NO adsorption[22]. When the relatively low temperature in the V/Sb/Ce/Ti (500s-1), this phenomenon significantly appears. This suggested that NO could be easily oxidized to NO_2 on the V/Sb/Ce/Ti (500s-1). These results were consistent with the Ce^{3+} ratio results by Ce 3d of XPS. Excellent SCR activity was achieved at higher Ce^{3+} ratio (Table 1). According to Chen et al.[34], surface adsorbed oxygen and Ce^{3+} may enhance the SCR reaction by promoting oxidation of NO to NO_2. NO oxidation ($NO + O_2$) experiments were performed to examine the influence of sulfation in V/Sb/Ce/Ti on the catalyst activity (Fig. 11). In the case of V/Sb/Ce/Ti (500s-1), the conversion of NO to NO_2 increased in a reaction from 200 to 400 °C. As the ratio of Ce^{3+} ratio increased in the surface of the catalysts treated with sulfation, the capacity for NO to NO_2 oxidation improved significantly. NO_2 production was highest with the use of V/Sb/Ce/Ti (500s-1). The oxidation of NO to NO_2 is now generally accepted to be an important reaction step to improve NOx reduction by NH_3 [35]. SCR catalysts having the capacity for NO to NO_2 oxidation exhibit excellent activity at low temperature due to the effects of 'Fast SCR'[36].

The O 1s peaks of the V/Sb/Ce/Ti catalysts by XPS are shown in Fig. 12. The O 1s peak was fitted into sub-bands by searching for the optimum combination of Gaussian bands. The sub-bands at 529.5–530.0 eV were attributable to the lattice oxygen O_2 (expressed by O_β)[13]. Two bands at 531.0–531.6 and 532.8–533.0 eV were assigned to the surface adsorbed oxygen (O_α), including O_2^{2-} and O belong to chemisorbed water (expressed as O'_α), respectively[37]. The O_α ratio (%) was calculated by $O_\alpha/(O_\alpha + O'_\alpha + O_\beta)$ of the V/Sb/Ce/Ti (Fresh). The O_α ratio (%) of the V/Sb/Ce/Ti (Fresh) was 38.25%. The O 1s peaks of the V/Sb/Ce/Ti catalysts were measured by XPS, the results of which are shown in Table 1. The O_α ratios (%) of the V/Sb/Ce/Ti (Fresh), V/Sb/Ce/Ti (250s-1), V/Sb/Ce/Ti (300s-1), V/Sb/Ce/Ti (400s-1), and V/Sb/Ce/Ti (500s-1) were calculated to be 38.25, 38.55, 44.11, 44.48, and 55.37%, respectively. This result showed enhancement as the surface chemisorbed oxygen was active in the SCR reaction[38]. The shift of the O 1s peak to a high binding energy proposed interaction between the lattice oxygen and metal atoms, which could be favorable for redox characteristic and the oxidation of NO to NO_2 in the SCR reaction[39]. According to Gu et al.[21], the surface chemisorbed oxygen of sulfated ceria is present much more as compared to CeO_2, reacting between adsorbed ammonia and activated oxygen was the key step for NH_3-SCR process. The higher ratios of surface chemisorbed oxygen in the sulfated catalysts could increase catalytic activity.

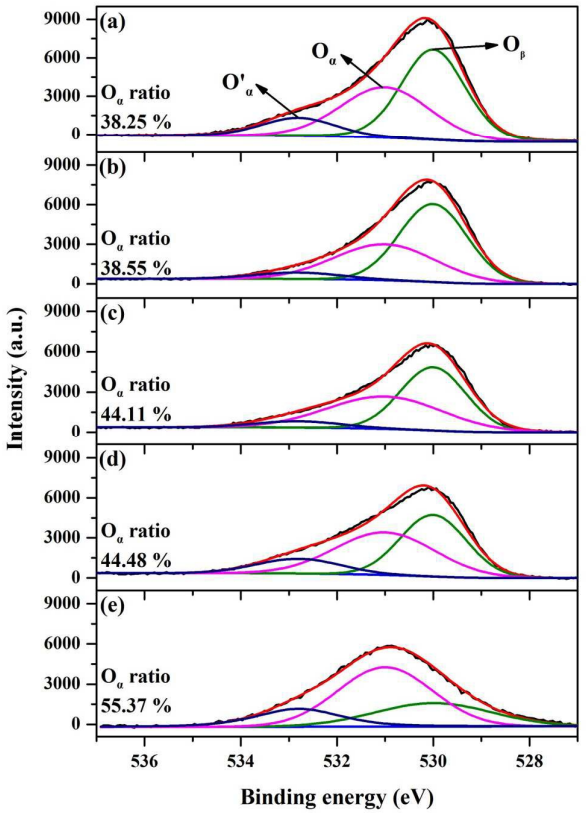

Fig. 12 The O 1s peaks of the V/Sb/Ce/Ti (Fresh) and sulfated V/Sb/Ce/Ti catalysts by XPS.

It was confirmed that the sulfate catalyst showed a positive effect on the catalytic activity through XPS, TPO, NH_3-TPD, DRIFTs, NO-TPD, and oxidation of NO to NO_2. Based on these results, causes of the increase in activity suggested through characterization of the sulfation treated catalysts are presented in Fig. 13. It was thought that the activity of the V/Sb/Ce/Ti (500s-1) was increased by the following 3 reactions: i) increase in NH_3 adsorption capacity through increase of the Brönsted and Lewis acid sites by the formation of SO_4^{2-} + NH_3 on the surface of the catalyst through sulfation. As NH_3 was adsorbed in SO_4^{2-} formed by cerium (III) sulfate species. The SO_4^{2-}–NH^{4+} was activated into SO_4^{2-}–NH_2, which then reacted with $NO_{(g)}$ for conversion into N_2 and H_2O, increasing the active sites. Thus, catalytic activity was improved. ii) in the sulfated catalyst, fast SCR reactions occurred due to the production of NO_2 through reaction of NO and O_2. The increase in the Ce^{3+} ratio of the sulfated catalyst had a positive effect on the increase in activity at low temperature through increase of the NO to NO_2 oxidation and redox properties. iii) it was determined that the exellent SCR activity by sulfation can be attributed to an enhancement in active oxygen species and chemisorption of NH_3. It was conducive to NH_3 activation. $NH_{3(g)}$ was adsorbed on the acid sites. $NH_{3(ad)}$ was then activated by surface adsorbed oxygen (activated oxygen) on the surface to form $–NH_2$. $–NH_2$ then reacted with the gaseous NO to form N_2 and H_2O. The sulfation treatment was beneficial for the formation of Ce^{3+} species. The presence of the Ce^{3+} species may cause a change imbalance. It means the vacancies and unsaturated chemical bonds on the catalysts surface[40], which will lead to the increase of surface adsorbed oxygen on the surface[32].

Topsøe et al.[29] suggested that the SCR reaction might take place through an Eley-Rideal and Langmuir-Hinshelwood models can coexist as dual model (ERLH) that is adsorbed ammonia reacts with NO in the gas phase or weakly adsorbed in the vanadium-titania based catalysts. The V/Sb/Ce/Ti (Fresh) follows the dual model (ERLH), since significant NO is adsorbed on the catalyst surface. On the other hand, in the case of sulfated catalysts, the absorption of NO is reduced[19]. Similarly, in this study, the adsorption of NO over V/Sb/Ce/Ti catalyst was restrained after the sulfation, which was consistent with the result of NO-DRIFTs and NO-TPD analysis. It suggests that the SCR reaction over sulfated CeO_2 mainly enhanced

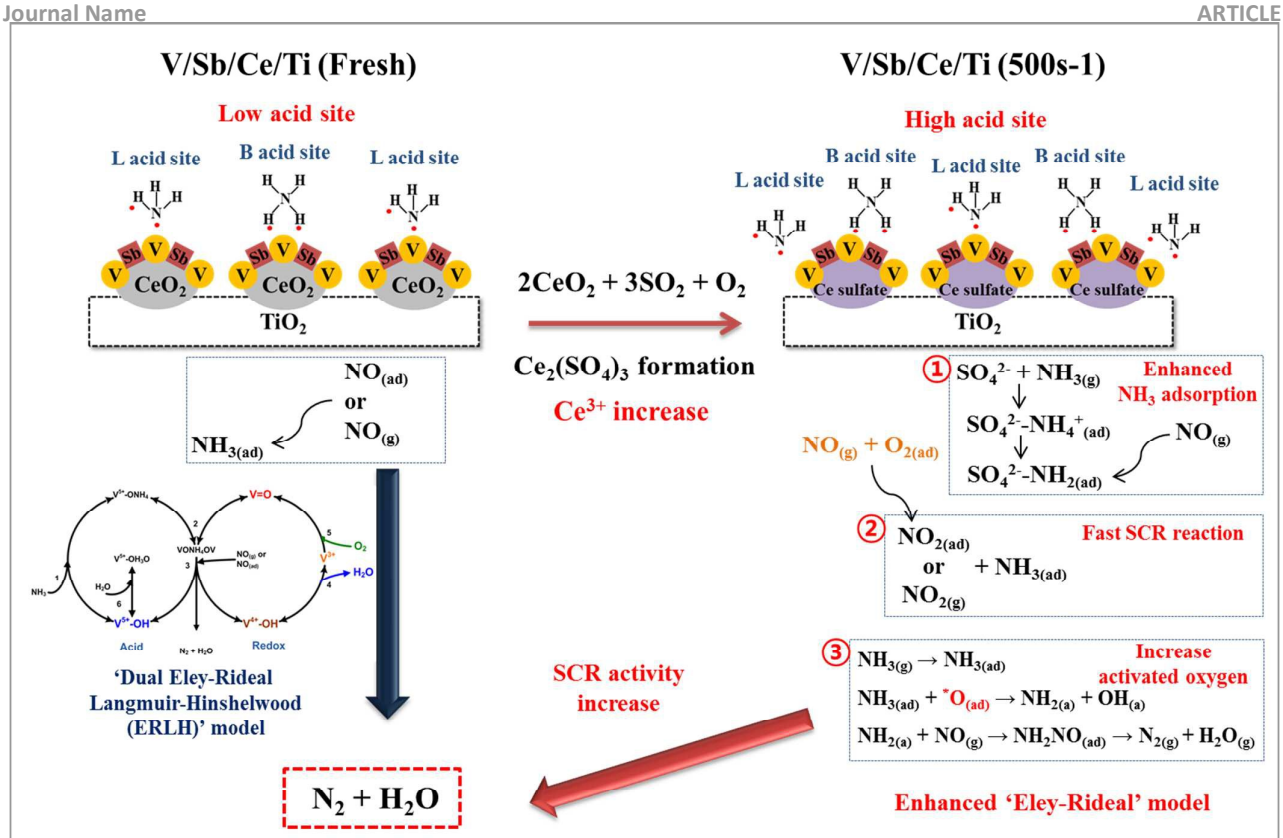

Fig. 13 Schematic expressed the cause of the increase in activity by sulfation in the V/Sb/Ce/Ti.

the Eley–Rideal mechanism (reaction of activated ammonia with gaseous NO)[21] as compared to the V/Sb/Ce/Ti (Fresh).

SO_2 deactivation.

The effects of SO_2 addition on the SCR of NO by NH_3 over the V/Sb/Ce/Ti (Fresh), V/Sb/Ce/Ti (500s-1), and V/W/Ti (Fresh) were monitored as a function of time on stream. The reaction conditions were as follows: 750 ppm NO, 48 ppm NO_2, NH_3/NOx=1.0, 3 vol.% O_2, 6 vol.% H_2O, 500 ppm SO_2, GHSV=60,000 h^{-1}, total flow rate 600 cc/min at 250 °C. All catalysts had the initial activity of 97%, which was almost equal. The activities were observed until they were reduced to 82% after deactivation. Fig. 14 shows the NOx conversion (%) depending on the reaction time for which SO_2 was present. The activity gradually decreased as SO_2 was injected into all catalysts. Activity of the catalysts was maintained in the following order before decrease to 82%: V/Sb/Ce/Ti (500s-1) (66 h) > V/Sb/Ce/Ti (Fresh) (58 h) > V/W/Ti (24 h). In the cases of V/Sb/Ce/Ti (500s-1) and V/Sb/Ce/Ti (Fresh), activity began to decrease 20 h after SO_2 was injected, at which the time point was similar. In addition, these catalysts showed superior SO_2 resistance as compared to V/W/Ti. In particular, the V/Sb/Ce/Ti (500s-1) demonstrated the best SO_2 resistance. This confirmed that the sulfation had effects on the improvement of SO_2 resistance.

The Ce valence states of the V/Sb/Ce/Ti (Fresh) and V/Sb/Ce/Ti (500s-1) were observed after the SO_2 resistance experiment. Increase of the Ce^{3+} ratio by the formation of $Ce_2(SO_4)_3$ had positive effects on the activity of the sulfated catalyst. A variety of literature[21] has claimed that the catalytic activity was increased by the formation of $Ce_2(SO_4)_3$. The Ce^{3+} ratio and NOx conversion at 250 °C before and after the SO_2 resistance experiment with V/Sb/Ce/Ti (Fresh) and V/Sb/Ce/Ti (500s-1) are shown in Table 2. Even if the activity of the V/Sb/Ce/Ti (Fresh) and V/Sb/Ce/Ti (500s-1) decreased after the SO_2 resistance experiment, the Ce^{3+} ratio was increased. This provided simple evidence to support the fact that the Ce^{3+} ratio did not have only a positive effect on the SCR reaction. The Ce^{3+} ratio was increased by injection of SO_2 in the sulfation and SO_2 deactivation experiment, but the activity showed quite different results. Thus, thermal gravimetric analysis (TGA), transmission infrared spectra (IR) and TPO analysis were performed to examine the effects of sulfation and the SO_2 resistance experiment.

Fig. 15 shows the TGA weight spectra. One peak at 600–720 °C was found for the V/Sb/Ce/Ti (Fresh) and V/Sb/Ce/Ti (500s-1). Small weight loss occurred in the V/Sb/Ce/Ti (Fresh) due to the evaporation of V_2O_5. The V/Sb/Ce/Ti (500s-1) had 3.84 wt.%, demonstrating a larger weight loss than the V/Sb/Ce/Ti (Fresh). Two weight loss steps could be observed for the deactivated V/Sb/Ce/Ti (500s-1) as peaks at 270–435 and 600–720 °C. The cause for decrease of the catalytic activity was the formation of ammonium sulfate in the SO_2 deactivation experiment. The peak at 270–435 °C was caused by the decomposition of $(NH_4)_2SO_4$ [41], while the peaks at 600–720 °C in the V/Sb/Ce/Ti (500s-1) and deactivated V/Sb/Ce/Ti (500s-1) corresponded to $Ce_2(SO_4)_3$. The V/Sb/Ce/Ti (500s-1) and deactivated V/Sb/Ce/Ti (500s-1) showed decreases of 3.84 and 4.62 wt.%, respectively. It was considered that the amount of $Ce_2(SO_4)_3$ was increased through the reaction of CeO_2 with SO_2 as the SO_2 deactivation experiment progressed. Weight loss by $Ce_2(SO_4)_3$ of the deactivated V/Sb/Ce/Ti (500s-1) was increased more than that of the V/Sb/Ce/Ti (500s-1). This corresponded to the increase in $Ce_2(SO_4)_3$ species by the SO_2 deactivation experiment.

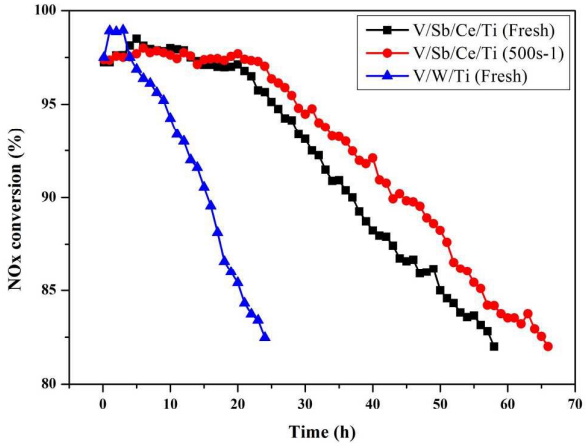

Fig. 14 Relative activity in the presence of SO_2 for the SCR of NO by NH_3 over V/Sb/Ce/Ti (Fresh), V/Sb/Ce/Ti (500s-1), and V/W/Ti (Fresh) at 250 °C (NO: 750 ppm, NO_2: 48 ppm, NH_3/NOx: 1.0, O_2: 3 vol.%, H_2O: 6 vol.%, SO_2: 500 ppm, GHSV: 60,000 h^{-1}).

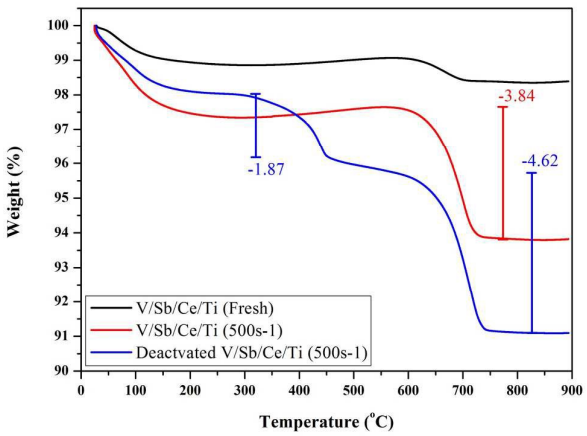

Fig. 15 TGA curves of V/Sb/Ce/Ti (Fresh), V/Sb/Ce/Ti (500s-1), and deactivated V/Sb/Ce/Ti (500s-1).

The transmission IR of the V/Sb/Ce/Ti (Fresh), V/Sb/Ce/Ti (500s-1), and deactivated V/Sb/Ce/Ti (500s-1) were shown in Fig. 16. For the deactivated V/Sb/Ce/Ti (500s-1), several bands at 982, 1128, 1196, 1414, and 1631 cm^{-1}, and a band around 3400–3500 cm^{-1} were detected. According to the literature[42], the strong bands at 1196 and 1128 cm^{-1} were caused by bulk sulfate species. The bands at 982 and 1414 cm^{-1} were due to the surface sulfate species, with only one S=O and three S–O bonds with the O atoms linked to the surface. The wide bands between 3400 and 3500 cm^{-1} and the band at 1631 cm^{-1} were assigned to H_2O[43]. It can be concluded that both surface and bulk sulfate species formed on the deactivated V/Sb/Ce/Ti (500s-1). The surface sulfate species corresponded to

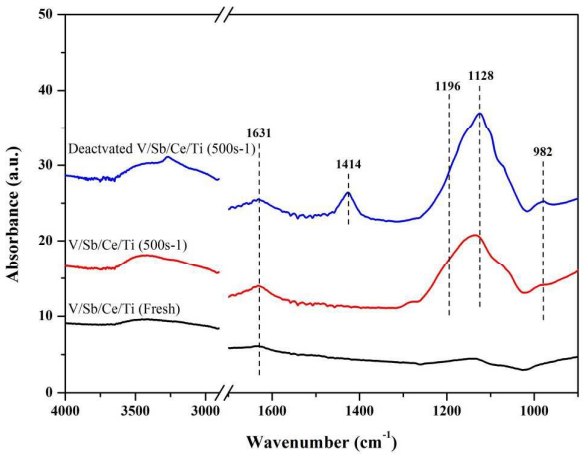

Fig. 16 Transmission IR spectra of V/Sb/Ce/Ti (Fresh), V/Sb/Ce/Ti (500s-1), and deactivated V/Sb/Ce/Ti (500s-1).

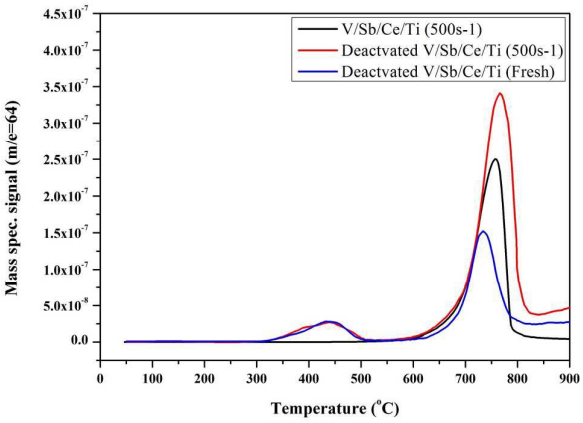

Fig. 17 TPO profiles of V/Sb/Ce/Ti (500s-1), deactivated V/Sb/Ce/Ti (500s-1), and deactivated V/Sb/Ce/Ti (Fresh) (Experimental conditions: 30 mg cat, 21% O_2/Ar oxidation with heating rate 10 °C /min, total flow rate 50 cm^3/min).

$(NH_4)_2SO_4$, formed by the SO_2 deactivation experiment. When compared with the V/Sb/Ce/Ti (Fresh) and V/Sb/Ce/Ti (500s-1), it was found that the strong bands at 1196 and 1128 cm^{-1} were formed, corresponding to $Ce_2(SO_4)_3$ of bulk sulfate species, and that such formation was caused by the sulfation. In addition, $Ce_2(SO_4)_3$ of bulk sulfate species seemed to increase after the SO_2 deactivation experiment of the V/Sb/Ce/Ti (500s-1).

The results of the TPO measurement of the V/Sb/Ce/Ti (500s-1), deactivated V/Sb/Ce/Ti (500s-1), and deactivated V/Sb/Ce/Ti (Fresh) are shown in Fig. 17. Peaks at 300–500 °C corresponding to $(NH_4)_2SO_4$ were observed for the deactivated V/Sb/Ce/Ti (500s-1) and deactivated V/Sb/Ce/Ti (Fresh). Peaks at 600–800 °C corresponding to $Ce_2(SO_4)_3$ were observed in all catalysts. Intensity of the peaks was related to the formation of cerium (III) sulfate species, which was found to be consistent with the Ce^{3+} ratio of each catalyst in Table 2. According to the SO_2 resistance experiment, cerium (III) sulfate species of the V/Sb/Ce/Ti (Fresh) and V/Sb/Ce/Ti (500s-1) increased.

The above results can be summarized as follows: the Ce^{3+} ratio of catalysts was increased due to the formation of $Ce_2(SO_4)_3$ through sulfation and the SO_2 deactivation experiment. Increase of the Ce^{3+} ratio by sulfation had a positive effect on catalytic activity. In contrast, the SO_2 deactivation experiment increased the Ce^{3+} ratio, but consequent SO_2 injection acted as a catalyst poisoning phenomenon due to the formation of $(NH_4)_2SO_4$. Therefore, SO_2 injection in the sulfation and SO_2 deactivation experiment had positive and negative effects on catalytic activity, respectively.

V/Sb/Ce/Ti (500s-5), V/Sb/Ce/Ti (500s-10), and V/Sb/Ce/Ti (500s-20) were prepared by increasing the sulfation time in order to examine the effects of Ce^{3+} ratio of sulfated catalyst on SCR activity and SO_2 resistance more clearly. The surface areas of the V/Sb/Ce/Ti (500s-5), V/Sb/Ce/Ti (500s-10), and V/Sb/Ce/Ti (500s-20) are collated in Table 2, where the values were 53.7, 45.1, and 41.6 m^2/g, respectively. The surface area was lower for V/Sb/Ce/Ti (500s-20). The surface area was gradually decreased, as sulfation time increases. The Ce^{3+} ratio and activity of V/Sb/Ce/Ti (500s-5), V/Sb/Ce/Ti (500s-10), and V/Sb/Ce/Ti (500s-20) at 250 and 200 °C can be seen in Table 2. The Ce^{3+} ratio was found to increase up to 58.41, 74.13, and 73.47%, respectively. Moreover, the Ce^{3+} ratios were higher than that of V/Sb/Ce/Ti (500s-1) (47.16%). When sulfation time was 10 h, the maximal Ce^{3+} ratio was obtained. Further increases were not observed for the 20 h. Activity at 250 and 200 °C was the same for all catalysts. Even if the Ce^{3+} ratio of the catalysts increased, further increase in the activity was not observed. The SO_2 deactivation experiment of V/Sb/Ce/Ti (500s-1), V/Sb/Ce/Ti (500s-5), V/Sb/Ce/Ti (500s-10), and V/Sb/Ce/Ti (500s-20) were also performed, the results of which are shown in Fig. 18. The initial activity was 97%, which was excellent. Reactions were observed until the activity decreased to 82% with SO_2 injections. The reaction times of the V/Sb/Ce/Ti (500s-5), V/Sb/Ce/Ti (500s-10), and V/Sb/Ce/Ti (500s-20) were 42, 27 and 25 h, respectively. These times were shorter than that of the V/Sb/Ce/Ti (500s-1) (65 h). Therefore, the SO_2 resistance of the V/Sb/Ce/Ti (500s-1) was the best. The increase in Ce^{3+} ratio showed high catalytic activity, but further increases did not occur when it exceeded a certain ratio. If the Ce^{3+} ratio was very high, SO_2 resistance decreased. Thus, the optimal conditions for sulfation were 1 h at 500 °C with consideration of the activity enhancement and SO_2 deactivation experiment.

Table 2 The surface area, Ce^{3+} ratio, and NOx conversion (at 250 and 200 °C) of various catalysts.

Catalyst	S_{BET} (m^2/g)	Ce^{3+} Ratio (%)	NOx conversion (%) at 250 °C	NOx conversion (%) at 200 °C
V/Sb/Ce/Ti (Fresh)	67.2	23.42	94.80	47.77
Deactivated V/Sb/Ce/Ti (Fresh)	-	41.35	82.00 (after SO_2 durability 58 h)	-
V/Sb/Ce/Ti (500s-1)	58.0	47.16	97.77	56.24
Deactivated V/Sb/Ce/Ti (500s-1)	-	73.16	82.00 (after SO_2 durability 66 h)	-
V/Sb/Ce/Ti (500s-5)	53.7	58.41	97.72	55.95
V/Sb/Ce/Ti (500s-10)	45.1	73.13	97.62	56.16
V/Sb/Ce/Ti (500s-20)	41.6	73.47	97.66	56.08

Experimental

Catalyst preparation.

V/W/Ti was prepared by wet impregnation of 2 wt.% vanadium and 5 wt.% tungsten on a prepared commercial TiO_2 (DT51, Cristal Global Co.). The required quantity of ammonium metavanadate (NH_4VO_3, Aldrich Chemical Co.) was added to an oxalic acid ($(COOH)_2$, Aldrich Chemical Co.) solution and heated to form an ammonium oxalate solution. V/Sb/Ti was prepared by wet impregnation of vanadium and 2 wt.% antimony on a prepared TiO_2 support. An aqueous solution of antimony was prepared using antimony acetate ($Sb(CH_3COO)_3$, Alfa Aesar). Ammonium metatungstate hydrate ($(NH_4)_6H_2W_{12}O_{40}$, Aldrich Co.) was used as W precursor. The mixed solution, in a slurry state, was then stirred for 1 h, after which the water was evaporated at 70 °C using a rotary vacuum evaporator (Eyela Co. N-N series). After water evaporation, the samples were dried for an additional 24 h at 103 °C in a dry oven to remove residual water. The samples were then calcined in air for 4 h at 400 °C.

V/Sb/Ce/Ti catalyst was prepared by wet impregnation of 2 wt.% vanadium and 2 wt.% antimony on a prepared Ce/Ti support. The required quantity of ammonium metavanadate was added to the oxalic acid solution and heated to form ammonium oxalate solution. An aqueous solution of antimony was prepared with

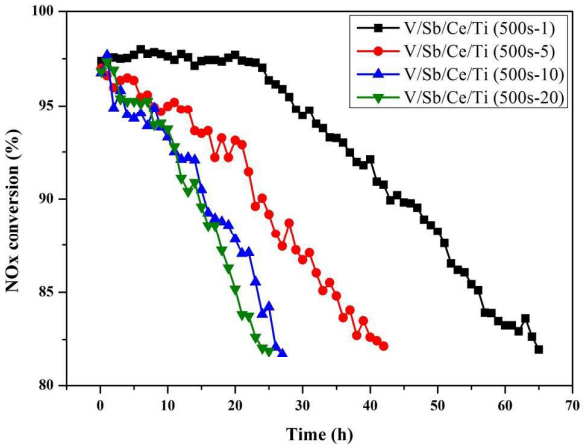

Fig. 18 Relative activity in the presence of SO_2 for the SCR of NO by NH_3 over V/Sb/Ce/Ti (500s-1), V/Sb/Ce/Ti (500s-10), and V/Sb/Ce/Ti (500s-20) at 250 °C (NO: 750 ppm, NO_2: 48 ppm, NH_3/NOx: 1.0, O_2: 3 vol.%, H_2O: 6 vol.%, SO_2: 500 ppm, GHSV: 60,000 h^{-1}).

antimony acetate. Both of the prepared solutions were added to a beaker containing a calculated amount of Ce/Ti powder; TiO_2 was combined with the solution by gradual stirring. The mixed solution, in a slurry state, was then stirred for 1 h, after which the water was evaporated at 70 °C using a rotary vacuum evaporator. After water evaporation, the samples were dried for an additional 24 h in a dry oven at 103 °C to remove any residual water. The sample was then calcined in air for 4 h at 500 °C. The Ce/Ti support was synthesized by the deposition precipitation method by hydrolysis with ammonium hydroxide (Aldrich, 25%)[44]. In the experiment, the required quantities of cerium (III) nitrate ($Ce(NO_3)_3{\cdot}6H_2O$, Aldrich Chemical Co.) (10 wt.% Ce) and commercial TiO2 powders were mixed together in water. Dilute aqueous ammonia was added to the mixture as a precipitating agent, and the resulting precipitate was filtered off. The obtained sample was dried for 24 h in a dry oven at 103 °C to remove residual water then calcined in air for 4 h at 500 °C[23].

To produce sulfated catalysts, the V/Sb/Ti and V/W/Ti catalysts (0.3 g) were treated with 800 ppm SO_2 and 3% O_2 with balance N_2 (total flow 600 cc/min) at 500 °C for 1 h. V/Sb/W/Ti was treated with 800 ppm SO_2 and 3% O_2 with balance N_2 at various temperatures (250, 300, 400 and 500 °C). The *x* and *y* in the *x*s-*y* catalyst were as follows: *x* = sulfation temperature, *y* = sulfation times (hours).

Test of catalytic activity.

The catalytic activity tests were carried out in a fixed-bed quartz reactor with an inner diameter of 8 mm. The reactant gases were fed to the reactor using a mass flow controller (MKS Co.) under the following reaction conditions: 750 ppm NO, 48 ppm NO_2, 800 ppm NH_3, 3 vol.% O_2, 6 vol.% H_2O, and 500 ppm SO_2 (when used) in Ar. Approximately 0.3 g of catalyst (40–50 mesh, 0.6 cc) was used for each test. Under ambient conditions, the total flow rate was 600 cc/min, with the hourly gas space velocity of 60,000 h^{-1}. The compositions of the feed gases and effluent streams were monitored continuously using on-line with non-dispersive infrared gas analyzers, as follows: ZKJ-2 (Fuji Electric Co.) for NO/NO_2; an Ultramat 6 (Siemens Co.) for N_2O; a pulsed fluorescence 43 C-High level gas analyzer (Thermo Co.) for SO_2; and NH_3 concentrations were measured using a detector tube (3M, 3La, 3L, GASTEC Co.). Before the gas flowed into the analyzers, moisture was removed using a moisture trap inside the chiller. The NOx conversion and rate constant were calculated from the concentrations of the gases at the steady state, according to the following equations:

$$\text{NOx conversion (\%)}=(([NO]_{in}-[NO+NO_2+2\times N_2O]_{out})/([NO]_{in}))\times 100 \quad (1)$$

$$NH_3 \text{ conversion (\%)}=(([NH_3]_{in}-[NH_3]_{out})/([NH_3]_{in}))\times 100 \quad (2)$$

Catalyst characterizations.

The BET surface areas of the catalysts were measured using ASAP 2010C (Micromeritics Co.). The specific surface area was estimated using the BET method, and the pore size of the distribution was calculated using the Barrett-Joyner-Halenda method that calculates the pore size based on the adsorption layer thickness in relation to the pressure and the average radius of the meniscus, as obtained using the Kelvin method. Each sample was then analyzed after degassing in a vacuum at 110 °C for 4 h.

An ESCALAB 210 (VG Scientific) was used for X-ray photoelectron spectroscopy (XPS) analysis, with monochromatic AlK_α (1486.6 eV) as the excitation source. After complete removal of moisture from the catalysts by drying at 100 °C for 24 h, analysis was performed without surface sputtering and etching so that the degree of vacuum in the XPS equipment was maintained at 10^{-6} Pa. Spectra were analyzed using XPS PEAK software (version 4.1). The intensities were estimated from the integration of each peak, subtraction of the Shirley background, and fitting of the experimental curve to a combination of Lorentzian and Gaussian lines of various proportions. All binding energies were referenced to the C 1s line at 284.6 eV. Binding energy values were measured with a precision of ±0.3 eV.

The temperature-programmed reduction (TPR) of H_2 was measured using 10% H_2/Ar and 0.3 g of the catalyst, at a total flow rate of 50 cc/min. Prior to the H_2 TPR measurements, the catalyst was pretreated in a flow of 5% O_2/Ar at 400 °C for 0.5 h, followed by cooling to 50 °C. The catalyst was placed in dilute hydrogen, and the consumption of hydrogen was monitored with an Autochem 2920 (Micrometrics) instrument while increasing the temperature to 800 °C at a rate of 10 °C/min.

Temperature programmed oxidation (TPO) measurements were carried out with 0.3 g samples of the catalysts under a total flow of 50 cc/min. The temperature increased from room temperature to 900 °C with heating rate of 10 °C/min under 21 vol.% O_2/Ar for the TPO. During the TPO experiments, the SO_2 (m/e 64) quantity was continuously monitored using a quadrupole mass spectrometer (QMS 422).

NH_3 temperature programmed desorption (TPD) measurements were carried out on 0.3 g samples of the catalysts under a total flow of 50 cc/min. Before the TPD measurements, the catalysts were pretreated in a flow of 5% O_2/Ar at 400 °C for 0.5 h then cooled to 50 °C. The samples were then treated with 1% NH_3/Ar for 1 h, after which the NH_3 was purged with Ar for 2 h before starting the TPD experiments. During the TPD experiments, the NH_3 (m/e 15) quantity was continuously monitored using a quadrupole mass spectrometer (QMS 422) while the temperature was increased to 600 °C at the rate of 10 °C/min.

This study used an in situ DRIFTs analysis performed with an FT-IR (Nicolet iS10, Thermo Co.). A DR (Diffuse Reflectance) 400 accessory was used for the analysis of the solid reflectance. The CaF_2 window was used as a plate for the DR measurement, and spectra were collected using a MCT (Mercury Cadmium Telluride) detector. All of the catalysts used for this analysis were ground using a rod in the sample pan of the in situ chamber with an installed temperature controller. To prevent the influence of moisture and impurities, the sample was preprocessed with Ar at a rate of 100 cc/min at 400 °C for 0.5 h. Then, the vacuum state was maintained using a vacuum pump. The spectra of the catalyst was collected by measuring the single-beam spectrum of the preprocessed sample as background, and all analyses were performed by auto scanning at a resolution of 4 cm^{-1}.

NO temperature programmed desorption (TPD) measurements were carried out on 0.3 g samples of the catalysts under a total flow of 50 cc/min. Before the TPD measurements, the catalysts were

pretreated in a flow of 5% O_2/Ar at 400 °C for 0.5 h then cooled to 50 °C. The samples were then treated with 1% NO/Ar for 1 h, after which the NH_3 was purged with Ar for 2 h before starting the TPD experiments. During the TPD experiments, the NO (m/e 30) and NO_2 (m/e 46) quantities were continuously monitored using a quadrupole mass spectrometer (QMS 422) while the temperature was increased to 600 °C at the rate of 10 °C/min.

TGA experiments were conducted using a thermo gravimetric analyzer (TGA) from TA instruments. The catalyst was loaded into the TGA reactor and purged with N_2 for 5 min. The temperature of the TGA furnace increased to 120 °C where it was maintained for 20 min to remove adsorbed water. The temperature was then increased to 900 °C at the rate of 10 °C min^{-1} in N_2.

The transmission IR spectra were obtained with a Nicolet Nexus spectrometer (Model Magna IR 550 II) equipped with a liquid nitrogen cooled MCT detector, for which 100 scans were collected with a spectral resolution of 4 cm^{-1}. The samples were mixed with KBr and pressed into pellets for testing.

Conclusions

The effects of sulfation of ceria added to V/Sb/Ti catalyst on the activity and SO_2 resistance were examined. Sulfation treatment was performed at 250, 300, 400, and 500 °C. The V/Sb/Ce/Ti (500s-1) demonstrated the best catalytic activity. As sulfate formed SO_4^{2-} on the surface of catalyst, total acidity increased, resulting in the increase in NH_3 adsorption capacity. After NH_3 was adsorbed on SO_4^{2-} and converted to SO_4^{2-}–NH_2, it further reacted with $NO_{(g)}$ to be converted into N_2 and H_2O, thereby resulting in excellent catalytic activity. In addition, as NO_2 was formed by the reaction of NO and O_2 in the sulfated catalyst, fast SCR reaction occurred. Increase in the surface Ce^{3+} ratio of the sulfated catalyst increased the NO to NO_2 oxidation and redox properties. The adsorption of NO over V/Sb/Ce/Ti catalyst was decreased after the sulfation treatment. It suggests that the SCR reaction by sulfation mainly enhanced the Eley-Rideal mechanism (reaction of activated ammonia with gaseous NO) as compared to the V/Sb/Ce/Ti (Fresh). Therefore, NOx conversion over the sulfated catalyst was superior to that over V/Sb/Ce/Ti (Fresh). Sulfation also increased the SO_2 resistance. However, SO_2 resistance decreased with increasing sulfation time. Sulfate of ceria had positive effects on catalytic activity, but excessive formation of cerium(III) sulfate species had negative effects on the SO_2 deactivation. The optimal conditions for sulfation were 1 h at 500 °C, with consideration of the activity enhancement and SO_2 deactivation in ceria added V/Sb/Ti catalyst.

Notes and references

1 P. Forzatti, *Appl. Catal. A*, 2001, **222**, 221–236.
2 L.J. Alemany, L. Lietti, N. Ferlazzo, P. Forzatti, G. Busca, E. Giamello and F. Bregani, *J. Catal*., 1995, **155**, 117–130.
3 G. Ramis, L. Yi, G. Busca, M. Turco, E. Kotur and R.J. Willey, *J. Catal*., 1995, **157**, 523–535.
4 F. Liu and H. He, *J. Phys. Chem. C*, 2010, **114**, 16929–16936.
5 K.H. Park, S.M. Lee, S.S. Kim, D.W. Kwon and S.C. Hong, *Catal. Lett.*, 2013, **143**, 246–253.
6 H. Huang, L. Jin, H. Lu, H. Yu and Y. Chen, *Catal. Commun.*, 2013, **34**, 1–4.
7 S. Zhang, H. Li and Q. Zhong, *Appl. Catal. A*, 2012, **435–436**, 156–162.
8 H.H. Phil, M.P. Reddy, P.A. Kumar, L.K. Ju and J.S. Hyo, *Appl. Catal. B*, 2008, **78**, 301–308.
9 L. Chen, J.H. Li and M.F. Ge, *J. Phys. Chem. C*, 2009, **113**, 21177–21184.
10 B.M. Reddy, A. Khan, Y. Yamada, T. Kobayashi, S. Loridant and J.C. Volta, *J. Phys. Chem. B*, 2003, **107**, 5162–5167.
11 W. Xu, Y. Yu, C. Zhang and H. He, *Catal. Commun.*, 2008, **9**, 1453–1457.
12 W.P. Shan, F.D. Liu, H. He, X.Y. Shi and C.B. Zhang, *Chem. Commun.*, 2011, **47**, 8046–8048.
13 W.P. Shan, F.D. Liu, H. He, X.Y. Shi and C.B. Zhang, *Appl. Catal. B*, 2012, **115–116**, 100–106.
14 X. Du, X. Gao, L. Cui, Y. Fu, Z. Luo and K. Cen, *Fuel*, 2012, **92**, 49–55.
15 B. Thirupathi and P.G. Smirniotis, *Appl. Catal. B*, 2011, **110**, 195–206.
16 L. Baraket, A. Ghorbel and P. Grange, *Appl. Catal. B*, 2007, **72**, 37–43.
17 X. Guo, C. Bartholomew, W. Hecker and L.L. Baxter, *Appl. Catal. B*, 2009, **92**, 30–40.
18 M.D. Amiridis, I.E. Wachs, G. Deo, J.M. Jehng and D.S. Kim, *J. Catal.*, 1996, **161**, 247–253.
19 S. Yang, Y. Guo, H. Chang, L. Ma, Y. Peng, Z. Qu, N. Yan, C. Wang and J. Li, *Appl. Catal. B*, 2013, **136–137**, 19–28.
20 W. Xu, H. He and Y. Yu, *J. Phys. Chem. C*, 2009, **113**, 4426–4432.
21 (a) T. Gu, Y. Liu, X. Weng, H. Wang and Z. Wu, *Catal. Commun.*, 2010, **12**, 310–313. (b) M.S. Maqbool, A.K. Pullura and H.P. Ha, *Appl. Catal. B*, 2014, **152–153**, 28–37.
22 H. Chang, L. Ma, S. Yang, J. Li, L. Chen, W. Wang and J. Hao, *J. Hazard. Mater.*, 2013, **262**, 782–788.
23 (a) D.W. Kwon, K.B. Nam and S.C. Hong, *Appl. Catal. B*, 2015, **166–167**, 37–44. (b) K.J. Lee, P.A. Kumar, M.S. Maqbool, K.N. Rao, K.H. Song and H. P. Ha, *Appl. Catal. B*, 2013, **142–143**, 705–717.
24 H. Fu, X. Wang, H. Wu, Y. Yin and J. Chen, *J. Phys. Chem. C*, 2007, **111**, 6077–6085.
25 P. Li, Q. Liu and Z. Liu, *Chem. Eng. J.*, 2012, **181–182**, 169–173.
26 S. Besselmann, C. Freitag, O. Hinrichsen and M. Muhler, *Phys. Chem. Chem. Phys.*, 2001, **3**, 4633–4638.
27 (a) J.G. Amores, V.S. Escribano, G. Ramis and G. Busca, *Appl. Catal. B*, 1997, **13**, 45–58. (b) G. Busca, L. Lietti, G. Ramis and F. Berti, *Appl. Catal. B*, 1998, **18**, 1–36.
28 N.Y. Topsoe, J. A. Dumesic and H. Topsoe, *J. Catal.*, 1995, **151**, 241–252.
29 N.Y. Topsoe, H. Topsoe and J. A. Dumesic, *J. Catal.*, 1995, **151**, 226–240.
30 Z.C. Si, D. Weng, X.D. Wu, J. Li and G. Li, *J. Catal.*, 2010, **271**, 43–51.
31 J. Laane and J.R. Ohlsen, *Prog. Inorg. Chem.*, 1980, **27**, 465–513.
32 L. Chen, J. Li and M. Ge, *Environ. Sci. Technol.*, 2010, **44**, 9590–9596.
33 Y. Liu, T. Gu, X. Weng, Y. Wang, Z. Wu and H. Wang, *J. Phys. Chem. C.*, 2012, **116**, 16582–16592.
34 L. Chen, J. Li, M. Ge and R. Zhu, *Catal. Today*, 2010, **153**, 77–83.
35 R.Q. Long and R.T. Yang, *J. Catal.*, 2000, **190**, 22–31.
36 (a) F. Liu and H. He, *Catal. Today*, 2010, **153**, 70–76. (b) E. Tronconi, I. Nova, C. Ciardelli, D. Chatterjee and M. Weibel, *J. Catal.*, 2007, **245**, 1–10.
37 (a) J.C. Dupin, D. Gonbeau, P. Vinatier and A. Levasseur, *Phys. Chem. Chem. Phys.*, 2000, **2**, 1319–1324. (b) J. Fang, X.

Bi, D. Si, Z. Jiang and W. Huang, *Appl. Surf. Sci.*, 2007, **253**, 8952–8961.
38 L.Q. Jing, Z.L. Xu, X.J. Sun, J. Shang and W.M. Cai, *Appl. Surf. Sci.*, 2001, **180**, 308–314.
39 (a) Q. Li, H. Yang, F. Qiu and X. Zhang, *J. Hazard. Mater.*, 2011, **192**, 915–921. (b) M. Kang, E.D. Park, J.M. Kim and J.E. Yie, *Appl. Catal. A*, 2007, **327**, 261–269.
40 S. Yang, W.P. Zhu, Z. Jiang, Z. Chen and J. Wang, *Appl. Surf. Sci.*, 2006, **252**, 8499–8505.
41 L. Mao, A.T. Raissi, C. Huang and N.Z. Muradova, *Int. J. Hydrog. Energy*, 2011, **36**, 5822–5827.
42 M. Waqif, P. Bazin, O. Saur, J.C. Lavalley, G. Blanchard and O. Touret, *Appl. Catal. B*, 1997, **11**, 193–205.
43 S. Lucas, E. Champion, D. Bregiroux, D. Bernache-Assollant and F. Audubert, *J. Solid State Chem.*, 2004, **177**, 1302–1311.
44 K.N. Rao, B.M. Reddy and S.E. Park, *Appl. Catal. B*, 2010, **100**, 472–480.

Graphical abstract